

Simultaneous odd- and even-order dispersion cancellation in quantum interferometry

Olga Minaeva,^{1,2} Cristian Bonato,^{1,3} Bahaa E.A. Saleh,¹ David S. Simon,¹ and Alexander V. Sergienko^{1,4}

¹ Dept. of Electrical & Computer Engineering, Boston University, Boston, Massachusetts 02215

² Department of Physics, Moscow State Pedagogical University, 119992 Moscow (Russia)

³ CNR-INFM LUXOR, Department of Information Engineering, University of Padova, Padova (Italy)

⁴ Dept. of Physics, Boston University, Boston, Massachusetts 02215

We describe a novel effect involving odd-order dispersion cancellation. We demonstrate that odd- and even-order dispersion cancellation may be simultaneously obtained in different regions of a single quantum interferogram using frequency-anticorrelated entangled photons and a new type of quantum interferometer. This offers new opportunities for quantum communication and metrology in dispersive media.

PACS numbers: 03.67.Bg, 42.50.St, 42.50.Dv, 42.30.Kq

INTRODUCTION

The even-order dispersion cancellation effect has been known in quantum optics for some time [1, 2]. It is based on nonclassical features of frequency-anticorrelated entangled photons. The nonlinear optical process of spontaneous parametric down conversion (SPDC) traditionally provides a reliable source of frequency-entangled photon pairs with anticorrelated spectral components. This condition comes as a consequence of energy conservation. If the frequency of the signal photon is ω_s , then the frequency of its twin idler photon must be $\omega_i = \Omega_p - \omega_s$, where Ω_p is the frequency of the pump beam. One of the traditional quantum interferometers records the modulation in the rate of coincidence between pulses from two photon-counting detectors at the output ports of a beamsplitter in response to a temporal delay between two spectrally correlated photons entering its input ports symmetrically. This type of quantum optics intensity correlation measurement, exhibited in the Hong-Ou-Mandel (HOM) interferometer [3], is manifested by an observed dip in the rate of coincidences. In previous demonstrations of dispersion cancellation, one photon of the downconverted pair travels through a dispersive material inserted in one arm of the HOM interferometer while its twin travels only through air. The final coincidence interference pattern (the dip) is not broadened in this case, demonstrating insensitivity to even-order dispersion coefficients [4].

Even-order dispersion cancellation has been used in quantum information processing, quantum communication, and in quantum optical metrology. For example, it enhances the precision of measuring photon tunneling time through a potential barrier [5] and improves the accuracy of remote clock synchronization [6]. The same effect provides superior resolution in quantum optical coherence tomography [7] by eliminating the broadening of interference envelope resulting from group velocity dispersion. The potential of quantum even-order dispersion cancellation has recently stimulated efforts to mimic this effect by use of classical nonlinear optical analogues [8, 9].

In this Letter we introduce a novel type of quantum interferometer that enables demonstration of the odd-order dispersion cancellation as a part of new dispersion management technique. In our design, both even-order and odd-order dispersion cancellation effects can be recorded as parts of a single quantum interference pattern.

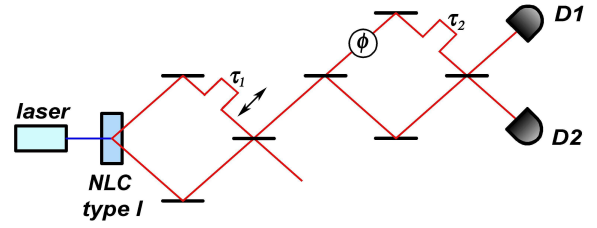


FIG. 1: Schematic diagram of the optical setup. The SPDC source produces pairs of frequency anticorrelated photons combined on a beamsplitter in a HOM interferometer configuration. Photons exiting one of the HOM interferometer ports are fed into a MZ interferometer and coincidence events are registered between two single-photon detectors at the output ports of the MZ interferometer. The dispersive sample generating phase delay (ϕ) is placed in one arm of a Mach-Zehnder interferometer.

HOM interferometers are commonly used to produce either $|\Psi\rangle \sim |2, 0\rangle - |0, 2\rangle$ state, when the delay τ_1 is set to balance the two paths, ensuring destructive interference in the middle of the interference dip, or a superposition of $|1, 1\rangle$, $|0, 2\rangle$ and $|2, 0\rangle$ states, when the delay τ_1 significantly unbalances two paths and shifts coincidences to the shoulder of HOM interference pattern. The performance of a Mach-Zehnder (MZ) interferometer fed by a particular quantum state has also been studied in detail [10].

In the new design, two interferometers work together in complete synergy. The setup consists of a HOM interferometer with one of its output ports providing input to a MZ interferometer. The state of light introduced into the MZ interferometer after the HOM interferometer is continuously modified when the delay τ_1 inside the HOM interferometer is scanned. The dispersive sample

providing a phase shift ϕ is placed in one arm of the MZ interferometer that is fed by a signal from one of the outputs of standard HOM interferometer, as illustrated in Fig.1. The delay τ_2 inside the MZ interferometer is kept at a particular fixed value. A peculiar quantum interference pattern can be observed in the rate of coincidences between two photon-counting detectors $D1$ and $D2$ at the output ports of the MZ interferometer as a function of τ_1 . The interference profile has two distinct patterns in this case. The central interference pattern depends only on the even-order dispersion coefficients, while the peripheral pattern depends only on the odd-order dispersion terms. This ability to manipulate and evaluate odd-order and even-order dispersion terms independently in a single quantum interferometer opens new perspectives in quantum communication and in precise optical measurement.

THEORETICAL MODEL

Assuming that detectors D_1 and D_2 are much slower than the temporal coherence time of the downconverted photons, the coincidence counting rate in such intensity correlation measurement is given by [11]:

$$R_c(\tau_1, \tau_2) = \int dt_1 \int dt_2 G^{(2)}(t_1, t_2), \quad (1)$$

where $G^{(2)}(t_1, t_2)$ is the second order correlation function defined by:

$$G^{(2)}(t_1, t_2) = |\langle 0 | \hat{E}_1^{(+)}(t_1) \hat{E}_2^{(+)}(t_2) | \Psi \rangle|^2. \quad (2)$$

$E_1^{(+)}(t_1)$ and $E_2^{(+)}(t_2)$ are the electrical field operators at the surfaces of detectors D_1 and D_2 , respectively.

$$\hat{E}_j^{(+)}(t_j) = \frac{1}{\sqrt{2\pi}} \int d\omega_j e^{-i\omega_j t_j} \hat{b}_j(\omega_j), \quad (3)$$

where $\hat{b}_j(\omega_j)$ is the mode operator at the corresponding detector, which may be expressed in terms of the input field operators $\hat{a}_j(\omega_j)$ [11]. The quantum state of light emitted in a frequency-degenerate non-collinear type-I phase-matching SPDC process with a monochromatic pump Ω_p is given by:

$$|\Psi\rangle \propto \int d\omega f(\omega) \hat{a}_1^\dagger(\Omega_0 + \omega) \hat{a}_2^\dagger(\Omega_0 - \omega) |0\rangle, \quad (4)$$

where $f(\omega)$ is a photon wavepacket spectral function defined by the phase matching condition in the nonlinear material, $\Omega_0 = \Omega_p/2$ is a central frequency of each wavepacket, $\omega_s = \Omega_0 + \omega$ corresponds to the signal photon frequency, and $\omega_i = \Omega_0 - \omega$ is a frequency of the idler photon of the down-converted pair.

The phase shift $\phi(\omega)$ acquired by the broadband optical wavepacket as it travels through a dispersive material could be expanded in a Taylor's series [12]:

$$\phi(\omega) = c_0 + c_1(\omega - \Omega_0) + c_2(\omega - \Omega_0)^2 + c_3(\omega - \Omega_0)^3 + \dots \quad (5)$$

where the linear term c_1 represents the group delay and the second-order term c_2 is responsible for group delay dispersion. In case of a conventional white-light interferometer, c_1 is responsible for a temporal shift of the interference pattern envelope, c_2 causes its temporal broadening, while c_3 provides a non-symmetric deformation of the wavepacket envelope. The higher-order terms might be included in consideration when a strongly dispersive material is used or in the case of extremely broadband optical wavepackets.

In the optical setup illustrated in Fig.1, the dispersive material providing the phase shift $\phi(\omega)$ could be situated in three possible locations in such layout. When a dispersive sample is placed in one of the arms of HOM interferometer it leads to the well-known even-order dispersion cancellation effect [4]. It may be easily shown that the presence of a dispersive material between the two interferometers does not affect the coincidence interferogram.

In this Letter we concentrate on the most interesting case when a dispersive sample producing the phase shift $\phi(\omega)$ is placed inside the MZ interferometer, the delay τ_2 is set to a particular fixed value, and the delay τ_1 is the variable parameter.

Following the usual formalism [11], one can show that the coincidence counting rate between detectors $D1$ and $D2$ is:

$$R_c(\tau_1, \tau_2) = \int d\omega (\Phi_0 - \Phi_\alpha(\omega, \tau_2) - \Phi_\beta(\omega, \tau_2)) \cdot (f(\omega)f^*(\omega) + f(\omega)f^*(-\omega)e^{-2i\omega\tau_1}), \quad (6)$$

where Φ_0 is a constant,

$$\Phi_\alpha(\omega, \tau_2) = e^{-2i\omega\tau_2} e^{i\phi(\Omega_0 - \omega)} e^{-i\phi(\Omega_0 + \omega)} + c.c., \quad (7)$$

and

$$\Phi_\beta(\omega, \tau_2) = e^{-2i\Omega_0\tau_2} e^{-i\phi(\Omega_0 - \omega)} e^{-i\phi(\Omega_0 + \omega)} + c.c. \quad (8)$$

Although not obvious from the form of equation (6), $R_c(\tau_1, \tau_2)$ is a real function for any shape of the spectrum $f(\omega)$. This can be seen by rewriting Eq. (6) in the more obviously real form:

$$R_c(\tau_1, \tau_2) = \int d\omega \{ |f(\omega)|^2 + |f(-\omega)|^2 + [e^{-2i\omega\tau_1} f(\omega)f^*(-\omega) + c.c.] \} \times [\Phi_0 - \Phi_\alpha(\omega) - \Phi_\beta(\omega)] \quad (9)$$

This ensures that the technique demonstrated here is applicable for all types of broadband frequency-anticorrelated states of light, including those with nonsymmetric spectral profiles produced using chirped periodically-poled nonlinear crystals.

The final coincidence counting rate $R_c(\tau_1, \tau_2)$ of Eq. (6) may also be written as a linear superposition:

$$R_c(\tau_1, \tau_2) = B + R_0(\tau_1) - R_{even}(\tau_1, \tau_2) - R_{odd}(\tau_1, \tau_2). \quad (10)$$

The first coefficient B incorporates all terms that are not dependent on the variable delay τ_1 , providing a constant after integration. It establishes a baseline level for the quantum interferogram. The following terms:

$$R_0(\tau_1) = 4 \int d\omega f(\omega) f^*(-\omega) e^{-2i\omega\tau_1}, \quad (11)$$

$$R_{even}(\tau_1, \tau_2) = \int d\omega f(\omega) f^*(-\omega) \cdot e^{-2i\omega\tau_1} [e^{-2i\Omega_0\tau_2} e^{-i\phi(\Omega_0-\omega)} e^{-i\phi(\Omega_0+\omega)} + e^{2i\Omega_0\tau_2} e^{i\phi(\Omega_0-\omega)} e^{i\phi(\Omega_0+\omega)}], \quad (12)$$

$$R_{odd}(\tau_1, \tau_2) = \int d\omega f(\omega) f^*(-\omega) \cdot [e^{-2i\omega(\tau_1+\tau_2)} e^{i\phi(\Omega_0-\omega)} e^{-i\phi(\Omega_0+\omega)} + e^{-2i\omega(\tau_1-\tau_2)} e^{-i\phi(\Omega_0-\omega)} e^{i\phi(\Omega_0+\omega)}] \quad (13)$$

are responsible for the shape of the interference pattern.

The term $R_0(\tau_1)$ represents a peak centered at $\tau_1 = 0$ that is simply a Fourier transform of the down converted radiation spectrum and is insensitive to the dispersion associated with $\phi(\omega)$. Since $R_{even}(\tau_1, \tau_2)$ is dependent on the sum $\phi(\Omega_0 - \omega) + \phi(\Omega_0 + \omega)$, it is sensitive to only even-order terms in the expansion Eq. (5). This manifests the odd-order dispersion cancellation effect and generates a dispersion-broadened function that is centered around $\tau_1 = 0$. The last term $R_{odd}(\tau_1, \tau_2)$, in contrast, is sensitive only to odd-order dispersion terms in $\phi(\omega)$. This term demonstrates the well known even-order cancellation. The coefficients $e^{-2i\omega(\tau_1+\tau_2)}$ and $e^{-2i\omega(\tau_1-\tau_2)}$ shift the two dips away from the center of the interference pattern in opposite directions. Such decomposition of quantum interference terms makes it possible to observe odd-order and even-order dispersion cancellation effects simultaneously in two distinct regions of the coincidence interferogram.

EXAMPLE

Our results are illustrated by a numerical example of quantum interference for a 3-mm thick slab of a strongly-dispersive optical material ZnSe, inserted in one arm of

the MZ interferometer to provide the phase shift $\phi(\omega)$. In this experiment we assume the use of frequency-entangled down-converted photons with 100-nm wide spectrum. As illustrated in Fig. 2, one can identify the narrow peak $R_0(\tau_1)$ in the center, which is insensitive to dispersion, along with the component $R_{even}(\tau_1, \tau_2)$, which is broadened by even-order dispersion contributions only. This central component of the interferogram illustrates the odd-order dispersion cancellation effect.

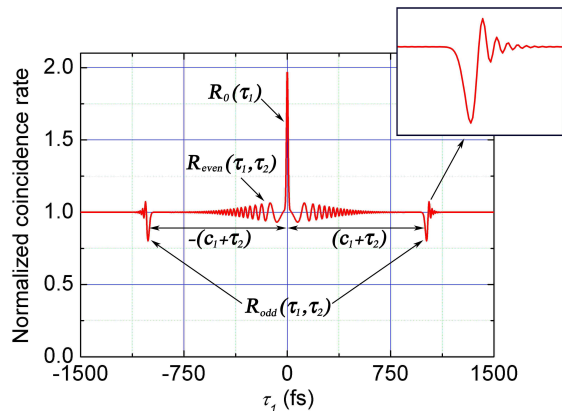


FIG. 2: The modulation of the normalized coincidence rate as a function of τ_1 delay when a 3-mm thick ZnSe sample is placed in the MZ interferometer. The fixed delay $\tau_2 = 26$ ps is used. The insert illustrates the odd-order dispersion contribution.

Two symmetric side dips $R_{odd}(\tau_1, \tau_2)$ appear shifted far away from the central peak by the group velocity delay c_1 acquired by entangled photons inside the dispersive material. However, this shift can be controlled by properly adjusting the value of the fixed delay τ_2 . Such a simple adjustment moves both dips back closer to the center and makes it convenient for observing both dispersion cancellation features in a single scan of the variable delay line (τ_1) inside HOM interferometer (see Fig. 2). The appearance of asymmetric fringes on the side of two dips is a clear sign of the third-order dispersion. [12].

DISCUSSION

This result can also be understood physically by analyzing all possible probability amplitudes that lead to measured coincidence events between $D1$ and $D2$. The input to the MZ interferometer is a pair of spectrally-entangled photons separated by a time delay τ_1 , i.e., if the leading photon has the high frequency, the lagging photon will have a low frequency, and vice-versa. We consider first the case when the dispersive element in the MZ interferometer arm is absent, so that the MZ interferometer introduces only a time delay τ_2 between its two arms. We also assume that τ_2 is much greater than the

width of the photon wave packet τ_c . To explain the features of the dependance of the photon coincidence rate on τ_1 , as shown in Fig.2, we consider three scenarios of processes occurring at the input ports of the second beam splitter of the MZ interferometer:

1) If $|\tau_1| > \tau_c$ and $|\tau_2 - \tau_1| > \tau_c$, then the two photons arriving at the ports of the final beam splitter will be distinguishable, so that no quantum interference is exhibited.

2) If $|\tau_1| \approx |\tau_2|$, so that $|\tau_2 - \tau_1| < \tau_c$, then quantum interference can occur when the leading photon takes the long path of the MZ interferometer and the lagging photon takes the short path, so that the two arrive almost simultaneously (within a time τ_c) at the two different ports of the final beam splitter. In this case, the Hong-Ou-Mandel (HOM) effect is exhibited at the beam splitter, albeit without full visibility because of the presence of the other possibility that both photons arrive at a single port, which leads to a background coincidence rate independent of τ_1 . From a different perspective, one may regard this scenario to be similar to that obtained in a Franson interferometer [13], for which photon pairs follow long-long or short-short paths. This scenario explains the components of the coincidence interferogram near $\tau_1 = \pm\tau_2$, and in this case the two spectrally-entangled photons entering separate ports of the final beam splitter lead to quantum interference accompanied by even-order dispersion cancellation.

3) Finally, when $|\tau_1| < \tau_c$, then one possibility is that the photons arrive at separate input ports of the final beam splitter. Since these photons are separated by a time $\tau_2 \gg \tau_c$, they are distinguishable and do not contribute to quantum interference. The other possibility is that the pair arrive at the same beam splitter input port. In this case, upon transmission or reflection at the beam splitter there are two alternatives for producing coincidence: transmission of the high-frequency photon and reflection of the low-frequency photon, or vice-versa. This explains the component of the coincidence interferogram near $\tau_1 \approx 0$. In this scenario, which involves two spectrally-entangled photons entering a single port of a beam splitter, quantum interference is accompanied by odd-order dispersion cancellation. We thus see that the quantum interference effects exhibited in scenarios 2) and 3) are accompanied by dispersion cancellation – although in opposite manners in the two cases.

In conclusion, we have demonstrated a new effect of odd-order dispersion cancellation and have shown that even- and odd-order dispersion cancellation may be simultaneously obtained in different regions of a quantum interferogram using a source of frequency-anticorrelated photons. This is accomplished by use of new quantum interferometer comprised a beamsplitter with variable

delay (HOM interferometer) followed by a single-input Mach-Zehnder interferometers with a fixed delay. The possibility of independently evaluating even-order and odd-order dispersion coefficients of a medium has the potential for applications in quantum communication and in quantum metrology of complex dispersive photonics structures. The demonstrated potential of even-order dispersion cancellation has recently stimulated the search for its classical analogues. [8, 9]. We expect that the scheme presented in this paper for simultaneous odd- and even-order dispersion cancellation would trigger the development of similar nonlinear optical techniques mimicking this quantum effect.

ACKNOWLEDGMENTS

We would like to thank Andrey Antipov from SUNY Buffalo for assistance with numerical simulations. This work was supported by a U. S. Army Research Office (ARO) Multidisciplinary University Research Initiative (MURI) Grant; by the Bernard M. Gordon Center for Subsurface Sensing and Imaging Systems (CenSSIS), an NSF Engineering Research Center; by the Intelligence Advanced Research Projects Activity (IARPA) and ARO through Grant No. W911NF-07-1-0629.

-
- [1] J. D. Franson, Phys. Rev. A **45**, 3126 (1992).
 - [2] A. M. Steinberg, P. G. Kwiat, and R. Y. Chiao, Phys. Rev. A **45**, 6659 (1992).
 - [3] C. K. Hong, Z. Y. Ou, and L. Mandel, Phys. Rev. Lett. **59**, 2044 (1987).
 - [4] A. Abouraddy, M. B. Nasr, B. E. A. Saleh, A. V. Sergienko, and M. C. Teich, Phys. Rev. A **65**, 053817 (2002).
 - [5] A. M. Steinberg, P. G. Kwiat, and R. Y. Chiao, Phys. Rev. Lett. **68**, 2421 (1992).
 - [6] V. Giovannetti, S. Lloyd, and L. Maccone, Nature **412**, 417 (2001).
 - [7] M. B. Nasr, B. E. Saleh, A. V. Sergienko, and M. C. Teich, Phys. Rev. Lett. **91**, 083601 (2003).
 - [8] B. I. Erkmen and J. H. Shapiro, Phys. Rev. A **74**, 041601 (2006).
 - [9] K. J. Resch, P. Puvanathan, J. S. Lunden, M. W. Mitchell, and K. Bizheva, Opt. Expr. **15**, 8797 (2007).
 - [10] R. A. Campos, B. E. A. Saleh, and M. C. Teich, Phys. Rev. A **42**, 4127 (1990).
 - [11] M. H. Rubin, Y. H. Shih, D. N. Klyshko, and A. V. Sergienko, Phys. Rev. A **50**, 5122 (1994).
 - [12] J.-C. Diels and W. Rudolph, *Ultrashort Laser Pulse Phenomena* (Elsevier Inc. and Academic Press, London, 2006).
 - [13] J. D. Franson, Phys. Rev. Lett. **62**, 2205 (1989).